

# Observational constraints on key-parameters of cosmic reionisation history

A. Gorce<sup>1,2</sup>, M. Douspis<sup>1</sup>, N. Aghanim<sup>1</sup>, and M. Langer<sup>1</sup>

<sup>1</sup> Institut d'Astrophysique Spatiale, Université Paris-Sud, CNRS, UMR8617, 91405 Orsay, France  
e-mail: agorce@ias.u-psud.fr

<sup>2</sup> Department of Physics, Blackett Laboratory, Imperial College, London SW7 2AZ, U.K.

Received \*\*\*\*\*, accepted \*\*\*\*\*

## ABSTRACT

We discuss constraints on cosmic reionisation and their implications on a cosmic SFR density  $\rho_{\text{SFR}}$  model; we study the influence of key-parameters such as the clumping factor of ionised hydrogen in the intergalactic medium (IGM)  $C_{\text{HII}}$  and the fraction of ionising photons escaping star-forming galaxies to reionise the IGM  $f_{\text{esc}}$ . Our analysis uses SFR history data coming from luminosity functions, assuming that star-forming galaxies were sufficient to lead the reionisation process at high redshift. We add two other sets of constraints: measurements of the IGM ionised fraction and the most recent result from Planck Satellite about the integrated Thomson optical depth of the Cosmic Microwave Background (CMB)  $\tau_{\text{Planck}}$ . We also consider various possibilities for the evolution of these two parameters with redshift, and confront them with observational data cited above. We conclude that, if the model of a constant clumping factor is chosen, the fiducial value of 3 often used in papers is consistent with observations; even if a redshift-dependent model is considered, the resulting optical depth is strongly correlated to  $C_{\text{HII}}$  mean value at  $z > 7$ , an additional argument in favour of the use of a constant clumping factor. Besides, the escape fraction is related to too many astrophysical parameters to allow us to use a complete and fully satisfactory model. A constant value with redshift seems again to be the most likely expression: considering it as a fit parameter, we get from the maximum likelihood (ML) model  $f_{\text{esc}} = 0.24 \pm 0.08$ ; with a redshift-dependent model, we find an almost constant evolution, slightly increasing with  $z$ , around  $f_{\text{esc}} = 0.23$ . Last, our analysis shows that a reionisation beginning as early as  $z \geq 14$  and persisting until  $z \sim 6$  is a likely storyline.

**Key words.** Cosmology: dark ages, reionisation, first stars – Cosmology: cosmic background radiation – Galaxies: high-redshift – Galaxies: evolution – Galaxies: formation

## 1. Introduction

Around redshift  $z \simeq 1090$ , during the recombination era, protons paired with free electrons to form neutral atoms: the ionisation level of the IGM fell to 0.0001 % and remained at this level for several billions of years (Peebles 1968; Zel'dovich et al. 1969; Seager et al. 2000). Yet, observations of the Gunn-Peterson effect (Gunn & Peterson 1965) in quasar spectra inform us that at  $z \sim 6$ ,  $99.96 \pm 0.03$  % of the IGM hydrogen atoms are ionised (Fan et al. 2006). What happened in the meantime, i.e. during the Epoch of reionisation (EoR), is an essential source of information about the evolution of the Universe, the formation of large cosmic structures and the properties of early galaxies, to cite only a few. Thanks to improved observations of the CMB, luminosity functions of galaxies, damping wings of quasars and Ly- $\alpha$  emissions (e.g. Schenker et al. 2013; Schroeder et al. 2013; Madau & Dickinson 2014; Planck Collaboration et al. 2016b), more and high quality data are available. Now the generally admitted storyline is that first star-forming galaxies reionised neutral regions around them between  $z \simeq 12$  and  $z \simeq 6$  and then the ionised regions progressively overlapped (e.g. Aghanim et al. 1996; Becker et al. 2015) so that IGM neutral hydrogen fraction rapidly decreased until quasars took over to reionise helium from  $z \simeq 3 - 4$  (Mesinger 2016).

Yet, some doubts remain about the sources of reionisation: some support the hypothesis that quasars could have led the process (Madau & Haardt 2015) but star-forming galaxies are often pre-

ferred. For instance, Robertson et al. (2015) argue that they were sufficient to maintain the IGM ionised at  $z \sim 7$ . The most recent value of the integrated Thomson optical depth, deduced from observations of the CMB, equals  $\tau_{\text{Planck}} = 0.058 \pm 0.012$  and is obtained considering an instantaneous reionisation at  $z_{\text{reio}} = 8.8 \pm 0.9$  ended by  $z = 6$  (Planck Collaboration et al. 2016b). It is much lower than previous observations by the Wilkinson Microwave Anisotropy Probe (WMAP)  $\tau_{\text{WMAP}} = 0.088 \pm 0.014$  for  $z_{\text{reio}} = 10.5 \pm 1.1$  (Hinshaw et al. 2013). This decrease, according to Robertson et al., reduces the need for a significant contribution of high-redshift galaxies and allows them to extrapolate galaxies luminosity functions for  $10 \lesssim z \lesssim 30$ .

Like Robertson et al. (2015), a number of recently published papers assume redshift-independent values of the escape fraction of ionising photons  $f_{\text{esc}}$  and of the clumping factor  $C_{\text{HII}}$  (Bouwens et al. 2015; Ishigaki et al. 2015; Greig & Mesinger 2017), which is a questionable hypothesis.  $f_{\text{esc}}$  depends on numerous astrophysical parameters and, for this reason, it is often a generalised, global and redshift-independent value that is used, for an order of magnitude of  $10^{-1}$ . Some simulations give expressions of  $f_{\text{esc}}$  as a function of redshift (Haardt & Madau 2012; Kuhlen & Faucher-Giguère 2012) or of various parameters such as halo mass or star formation rate (Wise et al. 2014; Paardekooper et al. 2015), but these models are rarely combined with observational constraints, aiming to deduce a certain history of reionisation. The situation is quite the same for the clumping

factor: its evolution with redshift can be considered in simulations through various models (e.g. Mellema et al. 2006; Pawlik et al. 2009; Sobacchi & Mesinger 2014), but these are rarely confronted to observations. We must however cite Price et al. (2016) who constrain parametrised models of the escape fraction  $f_{\text{esc}}(z)$  with Thomson optical depth and low multipole E-mode polarisation measurements from Planck Collaboration et al. (2016b), SDSS BAO data and galaxy observations for  $3 \lesssim z \lesssim 10$ .

We will first describe in Sec. 2 the observables of the reionisation process we will use throughout the analysis: the cosmic star formation rate density, the ionised fraction of the IGM and the Thomson optical depth, for which observational data is available – described in Sec. 3; as well as the two key-parameters of this study, the escape fraction of ionising photons and the clumping factor of IGM ionised hydrogen. Then, we look in Sec. 4 for the redshift-evolution we will further consider for the SFR density, extrapolating luminosity functions at  $z \gtrsim 10$ . Doing this, we study the impact of our observational constraints on  $\rho_{\text{SFR}}$ . Investigations are then made on the escape fraction value and on how observations can constrain it: we try several parametrisations out – a redshift-independent one, where  $f_{\text{esc}}$  is free to vary in  $[0.1, 0.4]$ , and a power-law function of  $z$ . We proceed the same for  $C_{\text{HII}}$ , but this time considering several possible parametrisations of its evolution with redshift, mainly from Iliev et al. (2007) and Pawlik et al. (2009). We conclude with a discussion on results in Sec. 5 and a summary in Sec. 6.

Throughout this paper, all cosmological calculations assume the flatness of the Universe and use the Planck cosmological parameters (Planck Collaboration et al. 2016a):  $h = 0.6774$ ,  $\Omega_{\text{m}} = 0.309$ ,  $\Omega_{\text{b}} h^2 = 0.02230$  and  $Y_{\text{p}} = 0.2453$ . Unless otherwise stated, all distances are comoving.

## 2. The observables of reionisation

### 2.1. Drawing the history of reionisation

Clues about the reionisation process can be derived from various observables. Under the assumption that star-forming galaxies provided the majority of the photons which ionised the IGM, the star formation rate density,  $\rho_{\text{SFR}}$ , can logically give precious information about the EoR. Eq. 1 relates  $\rho_{\text{SFR}}$  to the cosmic reionisation rate  $\dot{n}_{\text{ion}}$ , in units of photons per unit time per unit volume. Only a certain quantity of all photons produced by star-forming galaxies eventually end up ionising the IGM: first, they need to have sufficient energy, above the Ly- $\alpha$  limit, and second, they must escape their host galaxy and reach the IGM. The first condition is conveyed by the pre-factor  $\xi_{\text{ion}}$ , the quantity of Lyman continuum photons produced per second and per unit SFR for a typical stellar population.  $f_{\text{esc}}$ , the fraction of ionising radiation coming from stellar populations which is not absorbed by dust and neutral hydrogen within the host galaxy and so does contribute to the process, expresses the second condition. We use an averaged value for  $f_{\text{esc}} \xi_{\text{ion}}$  as the exact expression of  $\dot{n}_{\text{ion}}$  is an integral over magnitude (see Sec. 5.1).

$$\dot{n}_{\text{ion}} = f_{\text{esc}} \xi_{\text{ion}} \rho_{\text{SFR}}, \quad (1)$$

Aiming to reproduce observations on the star formation history, we choose a 4-parameter model suggested by Robertson et al. (2015), updated from Madau & Dickinson (2014, Sec. 5, Eq. 15) and described in Eq. 2 below. According to data,  $\rho_{\text{SFR}}(z)$  follows a first rising phase, over  $3 \lesssim z \lesssim 15$ , which will be expressed in our parametrisation by an evolution in  $\rho_{\text{SFR}}(z) \propto (1+z)^{b-d}$ , up to a peaking point around  $z \sim 1.8$  i.e. when the Universe was around 3.6 Gyr old. It then declines as  $\rho_{\text{SFR}}(z) \propto (1+z)^b$  until

$z = 0$ . To stay consistent with observations, we set  $b > 0$  and  $b - d < 0$ .

$$\rho_{\text{SFR}}(z) = a \frac{(1+z)^b}{1 + \left(\frac{1+z}{c}\right)^d}. \quad (2)$$

Other observations can lead to estimations of the fraction of ionised IGM  $Q_{\text{HII}}$ , also called filling factor, which relates to the SFR density via Eq. 3. In this equation, the time-related evolution of  $Q_{\text{HII}}$  depends on two contributions: an ionisation source term, proportional to  $\dot{n}_{\text{ion}}$ , and a sink term due to the competition of recombination.  $t_{\text{rec}}$  is the IGM recombination time defined in Eq. 4 and  $\langle n_{\text{H}} \rangle$  is the mean hydrogen number density, defined by  $\langle n_{\text{H}} \rangle = \frac{X_{\text{p}} \Omega_{\text{b}} \rho_{\text{c}}}{m_{\text{H}}}$ , with  $\rho_{\text{c}}$  the critical density of the Universe.

$$\dot{Q}_{\text{HII}} = \frac{\dot{n}_{\text{ion}}}{\langle n_{\text{H}} \rangle} - \frac{Q_{\text{HII}}}{t_{\text{rec}}}, \quad (3)$$

$$\frac{1}{t_{\text{rec}}} = C_{\text{HII}} \alpha_{\text{B}}(T) \left(1 + \frac{Y_{\text{p}}}{4X_{\text{p}}}\right) \langle n_{\text{H}} \rangle (1+z)^3. \quad (4)$$

In Eq. 4,  $X_{\text{p}}$  and  $Y_{\text{p}}$  are the primordial mass fraction of Hydrogen and Helium respectively.  $\alpha_{\text{B}}(T)$  is the case B recombination coefficient at a fiducial IGM temperature of  $T = 20\,000$  K, often considered as the mean temperature around a newly ionised atom. This value is consistent with measurements at  $z \sim 2 - 4$  (Lidz et al. 2010) but has been estimated to  $T \lesssim 10^4$  K at  $z \sim 5 - 6$  (Becker et al. 2011; Bolton et al. 2012). It fluctuates by a factor between 1 and 2, depending on the spectrum of the sources and on the time passed since reionisation (Hui & Haiman 2003). Yet,  $\alpha_{\text{B}}$  is expressed as  $\alpha_{\text{B}}(T) \approx 2.6 \times 10^{-13} T_4^{-0.76} \text{ cm}^3 \text{ s}^{-1}$  with  $T_4 = T/10^4$  K (Osterbrock 1989) i.e. is a weak function of  $T$  so that its variations do not affect our results significantly. Note that, rather than case A, we consider case B recombinations in order to exclude recombinations to the ground state and because we consider that ionisations and recombinations are distributed uniformly throughout the IGM, so that each regenerated photon soon encounters another atom to ionise (Loeb & Furlanetto 2013, Sec. 9.2.1). The clumping factor  $C_{\text{HII}}$  expresses how ionised hydrogen nuclei are distributed throughout the IGM.  $C_{\text{HII}}$  and  $t_{\text{rec}}$  are inversely proportional: the more the matter is aggregated in clumps, the easier for ionised atoms to recombine in these very same clumps.

To compare with the evolution derived from Eq. 3, we consider two parametrisations of the time evolution of the filling factor  $Q_{\text{HII}}$ , that we will then use to calculate the integrated Thomson optical depth from data. The first depicts the reionisation process as a step-like and instantaneous transition with a hyperbolic tangent shape (Eq. 5). The second is a redshift-asymmetric parametrisation, described in Eq. 6, inspired by Douspis et al. (2015). It uses a power-law defined by two parameters i.e. the redshift at which reionisation ends  $z_{\text{end}}$  and the exponent  $\alpha$ :

$$Q_{\text{HII}}(z) = \frac{f_{\text{e}}}{2} \left[ 1 + \tanh\left(\frac{y - y_{\text{re}}}{\delta y}\right) \right], \quad (5)$$

$$Q_{\text{HII}}(z) = \begin{cases} f_{\text{e}} & \text{for } z < z_{\text{end}}, \\ f_{\text{e}} \left(\frac{z_{\text{early}} - z}{z_{\text{early}} - z_{\text{end}}}\right)^{\alpha} & \text{for } z > z_{\text{end}}. \end{cases} \quad (6)$$

where  $y(z) = (1+z)^{\frac{3}{2}}$ ,  $y_{\text{re}} = y(z = z_{\text{re}})$  for  $z_{\text{re}}$  the redshift of instantaneous reionisation and  $\delta y = \frac{3}{2} (1+z)^{\frac{1}{2}} \delta z$ .  $z_{\text{early}}$  corresponds to the redshift around which the first emitting sources

form, and at which  $Q_{\text{H II}}(z)$  is matched to the residual ionised fraction ( $\bar{x} = 10^{-4}$ ). To be consistent with observations, which give  $Q_{\text{H II}}(z \leq 6.1) \simeq 1$  with very low uncertainty (McGreer et al. 2015; Fan et al. 2006), we choose  $z_{\text{end}} = 6.1$ . Furthermore, when comparing our findings with Planck results we set  $z_{\text{re}}$  equal to 8.8,  $z_{\text{early}} = 20$ , and also  $\alpha = 6.6$  (Planck Collaboration et al. 2016b).

Recent observations of satellites such as WMAP or Planck allow us to estimate the Thomson optical depth  $\tau$ , integrated over the electron column density to the Last Scattering Surface. It expresses the fraction of photons scattered along the line of sight by free electrons and thus is a direct indicator of the global ionisation rate of the IGM. It is related to the two previously described observables  $Q_{\text{H II}}$  and  $\rho_{\text{SFR}}$  via Eq. 7, where  $c$  is the speed of light in vacuum,  $\sigma_{\text{T}}$  the Thomson scattering cross-section,  $H(z)$  the Hubble constant and  $f_{\text{e}}$  the number of free electrons per Hydrogen nucleus. We assume that Helium is doubly ionised at  $z \leq 4$  (Kuhlen & Faucher-Giguère 2012) and thus have  $f_{\text{e}} = 1 + \eta Y_{\text{p}}/4X_{\text{p}}$  with  $\eta = 2$  for  $z \leq 4$  and  $\eta = 1$  for  $z > 4$ .

$$\tau(z) = c \langle n_{\text{H}} \rangle \sigma_{\text{T}} \int_0^z f_{\text{e}} \frac{Q_{\text{H II}}(z')}{H(z')} (1+z')^2 dz' \quad (7)$$

## 2.2. Configuring the key-parameters of reionisation

Among the various parameters cited in Sec. 2.1, two key-parameters of the reionisation history are still under a lot of investigations: the escape fraction and the clumping factor.

As mentioned before,  $f_{\text{esc}}$  expresses the fraction of the ionising radiation produced by stellar populations which is not absorbed by dust and neutral hydrogen within its host galaxy, and thus contributes to the ionisation of the IGM. In our approach, it is an effective value, averaged over stochasticity, halo mass dependencies in the source populations and, most importantly, over all sources considered in the Universe. This averaged value is hard to compare with observations of lone galaxies or haloes, which usually give much lower values. For instance, Steidel et al. (2001) and Iwata et al. (2009) estimate the escape fraction of some  $z \sim 3$  galaxies to be  $\geq 1\%$ . On the contrary, overall values of  $f_{\text{esc}}$  can be derived from simulations but are still highly uncertain. According to Finkelstein et al. (2015) and to agree with Ly- $\alpha$  forests measurements (Bolton & Haehnelt 2007), it should not be higher than 0.13; Fernandez et al. (2013) use a value of 0.1 from a simulation; Robertson et al. (2015) deduce from their analysis that, in order to have star-forming galaxies driving the reionisation process at high redshift,  $f_{\text{esc}}$  must equal at least 0.2. Last, Dunlop et al. (2013) assure that, considering the spectral energy distributions observed from high-redshift galaxies, it should be  $\approx 0.1-0.2$ . Yoshiura et al. (2017) summarise results on  $f_{\text{esc}}$  in these words: if it is generally acknowledged that, among all dependencies, the escape fraction decreases with the mass of the galaxy, there is a variance within 1 or 2 orders of magnitude among simulations results. For instance, a simulation from Yajima et al. (2014), on which assumptions of Robertson et al. (2015) are based, shows that, amidst all types of photons produced in star-forming galaxies (Ly- $\alpha$ , UV-continuum and ionising photons), the escape fraction of ionising photons is the only one which seems to depend neither on the redshift nor on the galaxy properties: it keeps a constant value of 0.2 with time, that we will use for our first analysis.

However, photons from different ranges of energy are subject to different physical phenomena and thus escape more or less easily from their host galaxy. For instance, dust extinguishes ionising, Ly- $\alpha$  and UV continuum photons similarly, but only ionising photons are also absorbed by neutral hydrogen clumps. Thus, at high redshifts, when there is few dust around the galaxy, photons of all energy ranges escape as easily; on the contrary, at low redshift, ionising photons experience more difficulties to escape than others (Yajima et al. 2014). We can then infer an increase of  $f_{\text{esc}}$  with redshift that we parametrise in Eq. 8, defined for  $z \geq 4$  and inspired by Kuhlen & Faucher-Giguère (2012). This evolution corresponds to either an evolution of the SFR of galaxies themselves and its associated feedback, or by a redshift evolution in the make up of the galaxy population. Here, owing to the UV spectral slope constraints, we set a maximum of 1 for the  $f_{\text{esc}}$  value, corresponding to a situation where all ionising photons escape.

$$f_{\text{esc}}(z) = \alpha \left( \frac{1+z}{5} \right)^{\beta} \quad (8)$$

In this parametrisation, also close to the one used in Price et al. (2016),  $\alpha$  is the value of  $f_{\text{esc}}$  at  $z = 4$  and  $\alpha\beta/5$  of its derivative at  $z = 4$ , redshift at which we expect the hydrogen ionising background to be dominated by star-forming galaxies (Kuhlen & Faucher-Giguère 2012). We take  $\beta$  positive in order to have an increasing escape with redshift, as anticipated earlier.

The second key-parameter of the reionisation process which we are going to investigate is the clumping factor of ionised hydrogen in the IGM  $C_{\text{H II}}$ , used in Eq. 4. It expresses how ionised hydrogen nuclei are gathered in heaps throughout the IGM. This parameter is essential because it is the growth of these clumps that allows the reionisation front to progress in the IGM and because competing recombinations will predominantly take place there. A precise estimate of  $C_{\text{H II}}$  can be difficult to obtain. Simulations have indeed several obstacles to overcome: getting a sufficient precision for the gas distribution, a correct topology of ionised and neutral matter, and an accurate model of the evolution of gas clumps themselves during the reionisation process. Besides,  $C_{\text{H II}}$  is often first defined on a single ionisation bubble and then summed on all bubbles to get the global volume-averaged value used here: the simulation must consider an extremely wide range of scales (Loeb & Furlanetto 2013, Sec. 9.2).

Most recent studies use values ranging from 1 to 6 at the redshifts of interest, i.e. for  $6 \lesssim z \lesssim 30$  (Sokasian et al. 2003; Iliiev et al. 2006; Raičević & Theuns 2011; Shull et al. 2012; Robertson et al. 2015; Finkelstein et al. 2015; Bouwens et al. 2015). Other studies predict a redshift-dependent evolution (Iliiev et al. 2007; Pawlik et al. 2009; Haardt & Madau 2012; Finlator et al. 2012; Sobacchi & Mesinger 2014), justified by the fact that during the late stages of EoR, ionisation fronts penetrate into increasingly overdense regions of the IGM, which have higher recombination rates and so drive a rapid increase of  $C_{\text{H II}}$  (Furlanetto & Oh 2005; Sobacchi & Mesinger 2014). In our studies, besides constant values of  $C_{\text{H II}}$ , we consider three parametrisations showing different evolutions with redshift for  $3 \leq z \leq 30$ <sup>1</sup>:

$$C_{\text{H II}}(z) = \alpha + a \left( \frac{z}{8} \right)^b, \quad (9)$$

$$C_{\text{H II}}(z) = \alpha + a \left( \frac{z}{8} \right)^b e^{c(z-8)}, \quad (10)$$

<sup>1</sup> We assume that  $C_{\text{H II}}$  is the same for H II and He III on this range.

$$C_{\text{HII}}(z) = a e^{b(z-8) + c(z-8)^2}. \quad (11)$$

The first two come from Pawlik et al. (2009) and are taken over in Haardt & Madau (2012). We update them in order to have  $a = C_{\text{HII}}(z = 8) - \alpha$  because  $z = 8$  is close to the redshift where  $Q_{\text{HII}} = 0.5$ . The third one comes from Mellema et al. (2006) and Iliev et al. (2007) and show a different behaviour compared to the first two. While the latter are strictly decreasing with  $z$ , this function is convex and has a minimum at  $z_{\text{min}} = -b/2c$ . As explained earlier, it is generally admitted that the clumping factor only decreases with  $z$ , and therefore we set  $z_{\text{min}} \gtrsim 30$  so that  $C_{\text{HII}}$  does not reach its minimum on our analysis range. For the same reason,  $a$  and  $b$  from Eq. 9 have to be of opposite signs and more precisely we take  $a > 0$  and  $b < 0$  in order to have  $C_{\text{HII}}(z) \xrightarrow{z \rightarrow 0} +\infty$ .

The definition of the clumping factor depends on the definition of the recombination time. If we consider an ionised proper volume  $V_p$  separated from the surrounding neutral gas by the ionisation front, we have  $t_{\text{rec}}^{-1} = \alpha_B (n_e V_p) n_{\text{HII}}$  where  $n_e V_p$  is the number of free electrons in the volume<sup>2</sup> (Strömgren 1939; Loeb & Furlanetto 2013). Generalising this result from  $V_p$  to the whole IGM gives:

$$\frac{1}{t_{\text{rec}}} = \alpha_B \langle n_e^2 \rangle \frac{(1+z)^3}{\langle n_{\text{H}} \rangle} = \alpha_B C_{\text{HII}} (1+z)^3 \langle n_{\text{H}} \rangle, \quad (12)$$

with  $C_{\text{HII}} = \langle n_{\text{HII}}^2 \rangle / \langle n_{\text{H}} \rangle^2$ . This equation corresponds to the previous definition of the recombination time given in Eq. 4 once  $f_e$  is introduced to account for the presence of He I in the IGM.

### 3. Data

The SFR density can be estimated via the observed infrared and rest-frame UV luminosity functions (LFs). We use the luminosity densities and SFR densities compiled by Robertson et al. (2015), computed from Madau & Dickinson (2014), Schenker et al. (2013), McLure et al. (2013), Oesch et al. (2015) and Bouwens et al. (2015). Robertson et al. also use HST Frontier Fields LF constraints at  $z \sim 7$  by Atek et al. (2015) and at  $z \sim 9$  by McLeod et al. (2015). Estimates of Madau & Dickinson (2014) derived from Bouwens et al. (2012) are updated with newer measurements by Bouwens et al. (2015). For the calculation of  $\rho_{\text{SFR}}$ , as a start, luminosity functions of star-forming galaxies are extended to UV absolute magnitudes of  $M_{\text{lim}} = -13$ . Then we compare with results for minimal and maximal magnitude limits  $M_{\text{lim}} = -17$  and  $M_{\text{lim}} = -10$ .

Observations related to the ionised fraction of the IGM  $Q_{\text{HII}}$  include the Gunn-Peterson optical depths and the dark-gap statistics measured in  $z \sim 6$  quasars (Fan et al. 2006; McGreer et al. 2015), damping wings measured in  $z \sim 6 - 6.5$  quasars (Schroeder et al. 2013) and the prevalence of Ly- $\alpha$  emission in  $z \sim 7 - 8$  galaxies (Schenker et al. 2013). They are listed in Bouwens et al. (2015).

Last, we consider estimations of the Thomson optical depth derived from Planck Satellite observations:  $\tau_{\text{Planck}} = 0.058 \pm 0.012$  for a redshift of instantaneous reionisation  $z_{\text{reio}} = 8.8 \pm 0.9$  (Planck Collaboration et al. 2016b); we will compare it to the asymptotic value  $\tau$  obtained from our model calculations at high redshift.

<sup>2</sup> As all the baryonic matter in the bubble  $V_p$  is by definition ionised and as we neglect the presence of helium, we have  $n_{\text{HII}} = n_{\text{H}} = n_e$ .

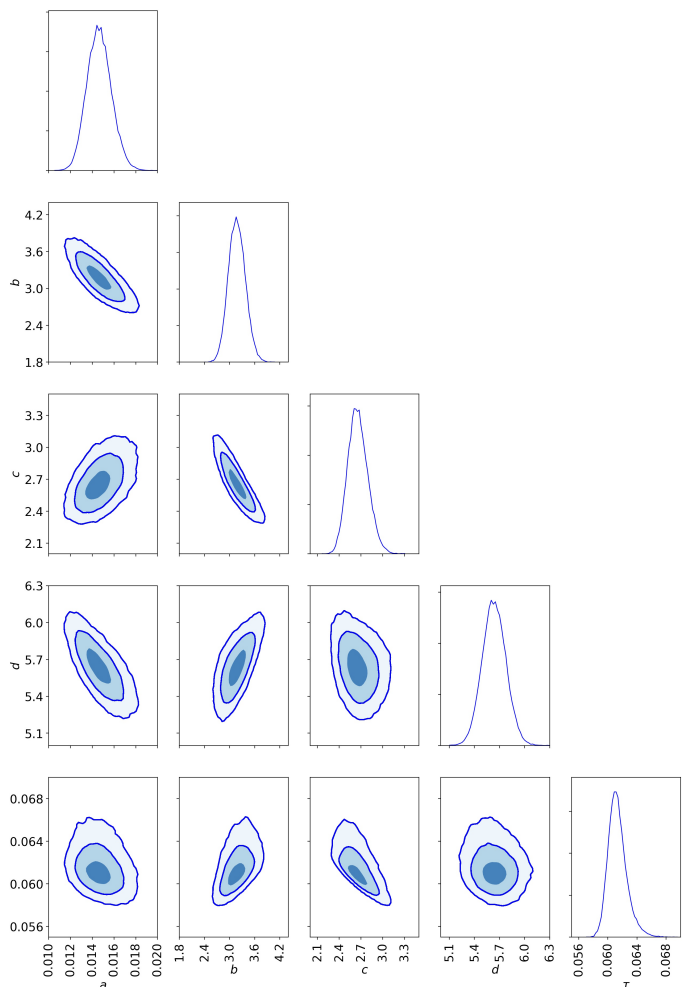


Fig. 1: Results of the MCMC analysis for the **ALL** case. The contours show the 1, 2, 3  $\sigma$  confidence levels for  $a, b, c, d$  and the derived parameter  $\tau$ .

## 4. Results

### 4.1. Cosmic star formation history

Since we are interested in the reionisation history both up to and beyond the limit of the current observational data, we adopt the four-parameter model from Eq. 2 into a Monte Carlo Markov chain approach. We perform a maximum likelihood (ML) determination of the parameter values assuming Gaussian errors on a redshift range of  $[0, 30]$ , extrapolating current observations on star formation history from  $z = 10.4$  to  $z = 30$ . We fit to the star formation data described in Sec. 3 and then compute the range of credible reionisation histories for every value of the  $\rho_{\text{SFR}}$  model parameters by solving the differential equation of Eq. 3. Filling factor data is used as an additional observational prior for the fit. Finally, we evaluate the Thomson optical depth as a function of  $z$  via Eq. 7 and compare its "asymptotic" value, at  $z = 30$ , to  $\tau_{\text{Planck}} = 0.058 \pm 0.012$  (Planck Collaboration et al. 2016b) as a last constraint on the fit. Because we want to know what observable constrains the reionisation history the most, all constraints are not always used: the run**ALL** uses all three sets of data as constraints; **NOQ** skips  $Q_{\text{HII}}$  data; **NORHO** skips star formation data and **ORHO** uses only SFR data in the fit.

In this first step, we adopt the fiducial, constant with redshift values  $f_{\text{esc}} = 0.2$ ,  $\log_{10} \xi_{\text{ion}} = 53.14$  [Lyc photons  $\text{s}^{-1} M_{\odot}^{-1} \text{yr}$ ] and

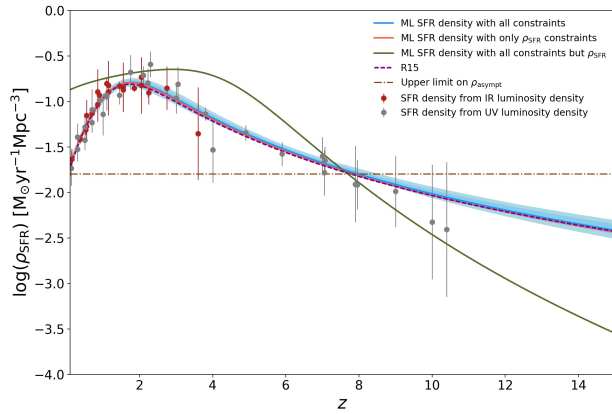


Fig. 2: Star formation rate density  $\rho_{\text{SFR}}$  with redshift. Data points are in red or blue depending on if they are determined from infrared (red) or ultraviolet (grey) luminosity densities – see Sec. 3 for details. Maximum likelihood parametrisations (continuous lines) are shown for various set of constraints: blue when all constraints are used; coral when only data on star formation are used; green when  $\tau$  and reionisation history data are used. The 68% confidence interval on  $\rho_{\text{SFR}}$  (light blue region) is drawn for the blue model. Note that the interval, corresponding to statistical uncertainties, is very narrow. These inferences are compared with a model forced to reproduce results from Robertson et al. (2015), cited as R15 in the legend, drawn as the purple dotted line. The horizontal dashed-dotted line corresponds to the upper limit on a hypothetical constant value of  $\rho_{\text{SFR}}$  for  $z > 10.4$  – see Section 5.3 for details.

$C_{\text{HII}} = 3$  (e.g. Pawlik et al. 2009; Shull et al. 2012; Robertson et al. 2013, 2015).

Results are summarised in Fig. 1 and in Table 1, and shown as well as in Fig. 2 for the star formation rate density and in Fig. 3 for the reionisation history. We find that it is the star formation history data that constrains reionisation history the most: both figures show that **ALL** and **ORHO** runs give similar evolutions and close ML values for  $a$ ,  $b$ ,  $c$  and  $d$  (see Table 3). Note that our constraints with **ORHO** and **ALL** are dominated by the data points at redshift  $\sim 5$  and the fixed functional form assumed for  $\rho_{\text{SFR}}(z)$ ; they are fully consistent with Robertson et al. (2015). On the contrary, for **NORHO**, the shape of  $\rho_{\text{SFR}}(z)$  is changed and reionisation begins much later, around  $z \sim 12$  rather than  $z \sim 15$  for other runs. **NORHO** results must be handled carefully as its parameters probability density functions (PDF) are extremely spread; the **NORHO** line drawn on figures corresponds to the median values of parameters. All we can conclude is that, when star formation history constraints are skipped, there is a much wider range of possible reionisation histories.

Table 1: ML model parameters for a model using all three sets of constraints.

a	b	c	d	$\tau$
0.1464	3.184	2.650	5.628	0.0615
$\pm 0.0011$	$\pm 0.206$	$\pm 0.137$	$\pm 0.144$	$\pm 0.0014$

Interestingly, Fig. 3 shows that for each run considering star formation history constraints, the process begins as early as  $z = 15$ . This is hardly compatible with WMAP results which stated that, if we consider reionisation as instantaneous, it should

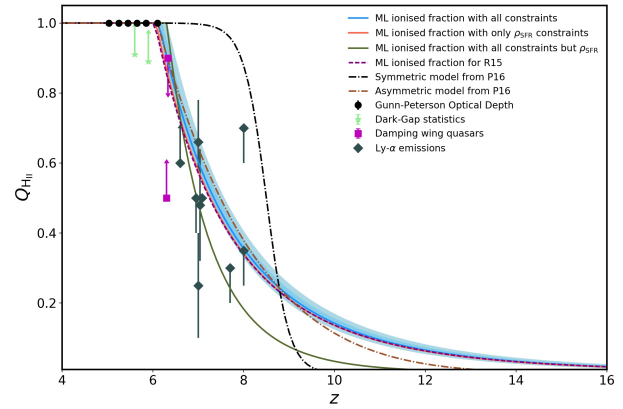


Fig. 3: Ionised fraction of the IGM  $Q_{\text{HII}}$  with redshift. Details on the origin of data points are given in the legend. ML models (continuous lines) are shown for various set of constraints: blue when all constraints are used, coral when only data on star formation are used, green when  $\tau$  and reionisation history data are used. The 68% confidence interval (light blue region) is drawn for the first model. Note that the interval, corresponding to statistical uncertainties, is very narrow. Inferences are compared with a model forced to reproduce results from Robertson et al. (2015), cited as R15 in the legend (dotted purple line) and with the two evolutions used in Planck Collaboration et al. (2016b, cited as P16) to model the reionisation process: a redshift-symmetric hyperbolic tangent as the brown dashed-dotted line and a redshift-asymmetric power-law in black.

occur at  $z_{\text{reio}} \approx 10.5 \pm 1.1$  (Hinshaw et al. 2013) and so cannot begin before  $z = 12$ . Observations also have an influence on the Thomson optical depth values, as **NORHO** gives a slightly lower value of  $\tau$  ( $0.053 \pm 0.003$  compared to  $0.062 \pm 0.001$  for **ALL**). Yet, all results remain in the  $1\text{-}\sigma$  confidence interval of  $\tau_{\text{Planck}}$ .

In the rest of the study we use the **ALL** run as our definitive parametrisation for  $\rho_{\text{SFR}}$  evolution with redshift: definitive parameters for Eq. 2 are ( $a = 0.1464$ ,  $b = 3.184$ ,  $c = 2.650$ ,  $d = 5.628$ ) from Table 1. ML parameters for other runs can be found in Table 3.

#### 4.2. The escape fraction of ionising photons $f_{\text{esc}}$

In order to study the role of the escape fraction in this analysis we choose, as detailed in Sec. 2.2, to first consider it as a fifth parameter of the fit, on top of ( $a$ ,  $b$ ,  $c$ ,  $d$ ) from Eq. 2. It is free to vary between 0 and 0.4. We name **ALL** the run which uses  $\rho_{\text{SFR}}$ ,  $Q_{\text{HII}}$  and  $\tau$  constraints, and **NOQ** the one that skips ionisation level constraints.  $f_{\text{esc}}$  is just involved in the  $\dot{n}_{\text{ion}}$  calculation of Eq. 1 and not in the one of  $\rho_{\text{SFR}}$  so that star formation history data take no part in the computation of  $f_{\text{esc}}$ . This explains why for all runs, results on the SFR density are close to the ones of Sec. 4.1 (see Tables 3 and 4 for details). For **ALL**, we get ML parameters ( $a = 0.0148$ ,  $b = 3.11$ ,  $c = 2.73$ ,  $d = 5.77$ ). Fig. 4 shows that  $Q_{\text{HII}}$  constraints have a strong influence on  $f_{\text{esc}}$ : confidence intervals are much wider for **NOQ** than for **ALL** (see Table 4). Besides, the **NOQ** PDF of  $f_{\text{esc}}$  is almost flat: standard deviation is equal to 0.079 i.e. around 30% of the mean value and two times more than for **ALL**. For now, we choose to use  $f_{\text{esc}} = 0.24 \pm 0.04$ , i.e. the mean value of the escape fraction for the **ALL** run, when a redshift-independent

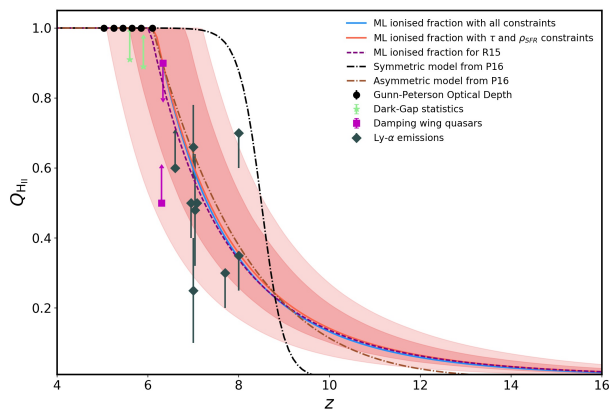


Fig. 4: Ionised fraction of the IGM  $Q_{\text{HII}}$  with redshift when  $f_{\text{esc}}$  is introduced as a parameter. Details on the origin of data points are given in the legend. ML models (continuous lines) are shown for various set of constraints: blue when all constraints are used, coral when  $Q_{\text{HII}}$  constraints are skipped, for which the 68% and 95% confidence intervals are drawn in salmon. These inferences are compared with a model forced to reproduce results from [Robertson et al. \(2015, R15, purple dotted line\)](#) and with the two evolutions used in [Planck Collaboration et al. \(2016b, P16\)](#): redshift-symmetric as the dashed-dotted brown line and redshift-asymmetric in black.

value is needed for  $f_{\text{esc}}$ . The full triangle plot for the **ALL** case is shown Fig. A.1 in Appendix.

We now turn to the possibility of a redshift evolution in  $f_{\text{esc}}$  for  $z \in [4, 30]$ . We perform a MCMC maximum likelihood sampling of the 2-parameter parametrisation described in Eq. 8. For the reasons explained above on the lack of relation between  $\rho_{\text{SFR}}$  and  $f_{\text{esc}}$ , we do not use star formation data as a constraint any more and assume that the time evolution of the SFR density follows Eq. 2 using parameters  $(a, b, c, d)$  resulting from Sec. 4.1. We use parameters corresponding to the set of constraints that is used on  $f_{\text{esc}}$ : if only  $\tau$  priors are considered here, we use  $(a, b, c, d)$  resulting from a **NOQ** run (see Table 3 for values).

We find that priors on the IGM ionisation level have a much stronger influence on results than the Thomson optical depth. Indeed, Fig. 5 shows that ML evolutions using both  $Q_{\text{HII}}$  and  $\tau$  constraints or only  $Q_{\text{HII}}$  are very similar: mean values for  $z \geq 4$  are similar by  $\sim 3\%$ . For **NOQ**, the optical depth remains surprisingly close to other models and higher than  $\tau_{\text{Planck}} = 0.058 \pm 0.012$ , around 0.064, but still in its  $1-\sigma$  confidence interval. The difference is visible on the storyline, as reionisation begins and ends later, around  $z = 6$  rather than  $z = 6.4$  in this case; on the contrary, when  $Q_{\text{HII}}$  data is used, the history tends to be the same as in previous analysis. Our results when only  $\tau_{\text{Planck}}$  constraints are considered are quite similar to those of [Price et al. \(2016\)](#) in which authors study the evolution of  $f_{\text{esc}}$  with redshift. They mainly use constraints from  $\tau_{\text{Planck}}$  but not from  $\rho_{\text{SFR}}$  which we have however found to be the most constraining set of data on reionisation history, concluding to a strong increase of  $f_{\text{esc}}$  from about 0.15 to about 0.55, depending on the observational constraints used.

ML parameters for Eq. 8 when all constraints are considered are  $(\alpha = 0.177 \pm 0.021, \beta = 0 \pm 0.22)$  and give a mean value for  $f_{\text{esc}}$  of 0.23, which is extremely close to the  $0.24 \pm 0.04$  found when considering the escape fraction constant with redshift (see

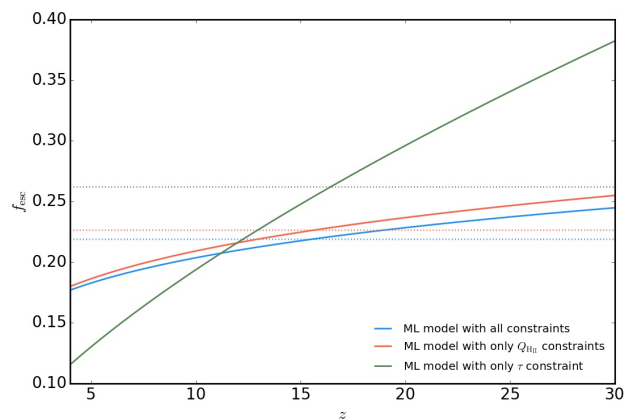


Fig. 5: Possible evolutions of  $f_{\text{esc}}$  with redshift. ML models are shown for various set of constraints: blue when all constraints are used; coral when  $\tau$  constraints are skipped; green when  $Q_{\text{HII}}$  constraints are skipped. Horizontal dotted lines represent the mean value of  $f_{\text{esc}}$  over  $4 \leq z \leq 30$  for the model of the corresponding colour.

Table 4 for details).

#### 4.3. The clumping factor of ionised hydrogen in the IGM $C_{\text{HII}}$

Following the definition of Sec. 2.2, we now investigate the constraints on  $C_{\text{HII}}$  set by observations. As we did in Sec. 4.2 for  $f_{\text{esc}}$ , we add  $C_{\text{HII}}$  as a fifth parameter of the fit on  $\rho_{\text{SFR}}$  using Eq. 2, apart from  $(a, b, c, d)$ . It is free to vary between 0 and 10, the order of magnitude of fiducial values mainly used in publications (e.g. [Shull et al. 2012; Robertson et al. 2013, 2015](#)). Here again, we call **ALL** the run using all constraints in the fit, and **NOQ** the one that skips  $Q_{\text{HII}}$  constraints.

After performing the MCMC ML sampling of the 5 parameters (see Table 4 for details), we get a quite spread PDF for  $C_{\text{HII}}$  with **ALL**: the standard deviation is equal to 1.39 for a median value of 2.70 and a mean value of 2.84. Even with such a wide range of possible values, the range of possible reionisation histories remains very narrow and the Thomson optical depth PDF is almost exactly the same as when we take  $C_{\text{HII}} = 3$ :  $\tau_{\text{ALL}} = 0.0614 \pm 0.0014$  to compare with  $\tau_{C_{\text{HII}}=3} = 0.0615 \pm 0.0014$  (see Table 2 and Fig. A.2 in Appendix). Besides, for **NOQ**, reionisation ends later – around  $z = 5.8$  – and  $\tau$  takes lower values ( $\tau_{\text{NOQ}} = 0.0595 \pm 0.0071$ ) but remains, as others, in the  $1-\sigma$  confidence interval of  $\tau_{\text{Planck}}$ . This confirms that IGM ionisation level data are compatible with Planck observations and that the value of  $C_{\text{HII}}$  constrains only slightly the reionisation history.

Now, we will successively test the three redshift-dependent models of the clumping factor given in Eq. 9, 10 and 11.  $C_{\text{HII}}$  is not involved in the calculation of  $\rho_{\text{SFR}}$  but only of the recombination time, and so in the differential equation allowing us to compute  $Q_{\text{HII}}$  and then  $\tau$ . Thus, as for  $f_{\text{esc}}$ , star formation history data have no influence over it: the **ALL** run is now constrained by  $Q_{\text{HII}}$  and  $\tau_{\text{Planck}}$  only. It is also important to notice that, for low values of  $z$  (precisely for  $z \leq 6.8$ ),  $Q_{\text{HII}}$  becomes higher than 1 in our calculations, which is physically irrelevant. To take this into account, we set arbitrarily  $Q_{\text{HII}} = 1$  for  $z \leq 6.8$ . Values of

Table 2: Resulting Thomson optical depths for various evolutions of  $C_{\text{HII}}$  with redshift.

Model	$\langle \tau \rangle$	$\sigma$
$C_{\text{HII}} = 3$	0.0615	0.0014
Free	0.0614	0.0014
HM12.1	0.0606	0.0021
HM12.2	0.0612	0.0015
I07	0.0635	0.0018

**References.** Free: Model with  $C_{\text{HII}}$  as a fifth parameter, varying in [1, 10]; HM12.1 & HM12.2: [Haardt & Madau \(2012\)](#), respectively Eq. 9 and 10; I07: [Iliev et al. \(2007\)](#), Eq. 11.

$C_{\text{HII}}(z)$  in the parametrisations at low redshift are thus irrelevant in this study.

Once again, IGM reionisation level data constrain results more than  $\tau_{\text{Planck}}$ . The redshift-evolution of  $C_{\text{HII}}$  and  $Q_{\text{HII}}$  for the three parametrisations presented in Sec. 2.2 and for **ALL** runs are shown on Figs. 6 and 7. We see on the first figure that there are a lot of possible output evolutions for the first model as grey lines are extremely spread but this does not translate in significant variations of  $Q_{\text{HII}}(z)$  whose 68% confidence interval – drawn as a blue region – is on the contrary very narrow. All storylines remain quite close, with a beginning around  $z = 20$  and an end at  $z = 6.1$ , i.e. slightly later than previously. This means that, as in previous paragraph where  $C_{\text{HII}}$  was assumed constant with redshift, its exact value has no significant impact on the reionisation history. Besides, for the first two parametrisations, at  $z > 10$ ,  $C_{\text{HII}}(z)$  remains very close to its mean value (dotted horizontal line) and experiences little variations. In fact, variations in  $C_{\text{HII}}$  have more impact on the computed Thomson optical depth than on  $Q_{\text{HII}}$ : as detailed in Table 2, the third parametrisation gives a higher value of  $\tau$  than the two others, for a lower mean value of the clumping factor – what is consistent with Eqs. 4 and 7. All values remain though in the 1- $\sigma$  confidence interval of  $\tau_{\text{Planck}}$ .

Finally, it seems like the fiducial constant value often used in papers, i.e.  $C_{\text{HII}} = 3$ , and which lies between the mean values of our models ( $\sim 4.15$  for the first two and 2.40 for the third, see Table 4), is a reasonable choice. More generally, and in accordance with [Bouwens et al. \(2015\)](#), as long it remains in a range of [0.5, 6.0], which is the 95% confidence interval of  $C_{\text{HII}}$  from first paragraph, results are consistent with the three sets of constraints available. This result is corroborates the work of [Price et al. \(2016\)](#), who also note that their analysis is almost completely independent of the clumping factor over the prior range  $1 < C_{\text{HII}} < 5$ .

#### 4.4. Varying both $f_{\text{esc}}$ and $C_{\text{HII}}$

Now we have studied the impact of  $f_{\text{esc}}$  and  $C_{\text{HII}}$  separately, we set the evolution of  $\rho_{\text{SFR}}(z)$  according to Eq. 2, using parameters  $a$ ,  $b$ ,  $c$  and  $d$  resulting from the analysis of Sec. 4.1. We perform a MCMC maximum likelihood sampling of the two parameters  $f_{\text{esc}}$  and  $C_{\text{HII}}$ , considered constant with redshift. We constrain the fit with filling factor data and  $\tau_{\text{Planck}}$ . The first is allowed to vary between 0.001 and 1, the other between 1 and 7. We show parameter distributions for  $f_{\text{esc}}$  and  $C_{\text{HII}}$  on Fig. 8.

If we consider the median value of each parameter distribution as its maximum likelihood value, we find  $f_{\text{esc}} = 0.230 \pm$

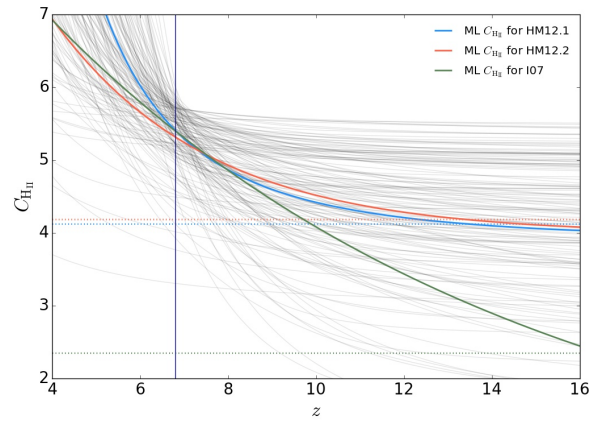


Fig. 6: Possible evolutions of  $C_{\text{HII}}$  with redshift. ML models are shown for the three models of Sec. 2.2: blue for the first, coral for the second and green for the third. Dotted horizontal lines correspond to the mean value of  $C_{\text{HII}}(z)$  for  $z > 6.8$ , where outputs of the model are used in calculations, for the model of the corresponding colour. The vertical dark blue line is located at  $z = 6.8$ . Grey lines represent various outputs of the sampling of the first model. **References.** HM12.1 & HM12.2: [Haardt & Madau \(2012\)](#), Eq. 9 and 10 in this paper. I07: [Iliev et al. \(2007\)](#), Eq. 11 in this paper.

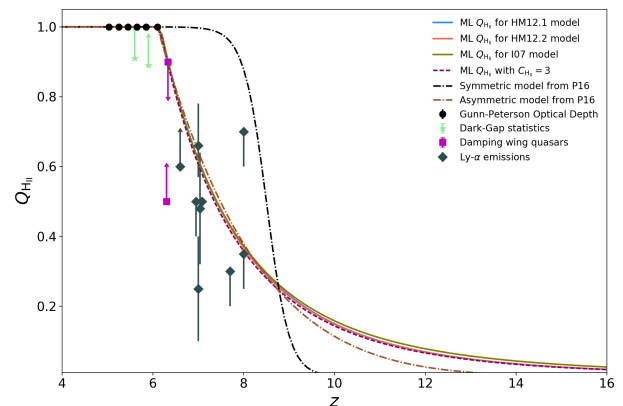


Fig. 7: Redshift evolution of  $Q_{\text{HII}}$  for various corresponding models of  $C_{\text{HII}}(z)$  in Sec. 2.2: blue for the first, with a blue region for the corresponding 68% confidence interval; coral for the second and green for the third. Inferences are compared to a result with  $C_{\text{HII}}(z) = 3$  in purple dashed line, and to the theoretical models of [Planck Collaboration et al. \(2016b\)](#): a redshift-symmetric model in black and a redshift-asymmetric model in brown. **References.** HM12.1 & HM12.2: [Haardt & Madau \(2012\)](#), Eq. 9 and 10; I07: [Iliev et al. \(2007\)](#), Eq. 11; P16: [Planck Collaboration et al. \(2016b\)](#).

0.025 and  $C_{\text{HII}} = 4.60 \pm 1.08$ . We see results are pretty similar to the previous analysis: if the escape fraction is well constrained, with a standard deviation of about 10%, the clumping factor can take a much wider range of values, between 2 and 6. Note that there seems to be a strong upper bound for the escape fraction around 0.26, which we can compare to the asymptotic value of  $f_{\text{esc}}$  when it is allowed to change with redshift (see Fig. 5). Because parameters take values close to the fiducial ones used in

Table 3: ML parameters from the fit on  $\rho_{\text{SFR}}$  with various parameters and constraints.

Ref.	Constraints			$\rho_{\text{SFR}}$ model				Other parameters	
	$\rho_{\text{SFR}}$	$Q_{\text{HII}}$	$\tau_{\text{Planck}}$	$a$	$b$	$c$	$d$	$f_{\text{esc}}$	$C_{\text{HII}}$
ALL	✓	✓	✓	$0.0146 \pm 0.0011$	$3.18 \pm 0.21$	$2.65 \pm 0.14$	$6.63 \pm 0.14$	–	–
NORHO	✓	✗	✗	$0.0146 \pm 0.0011$	$3.21 \pm 0.22$	$2.63 \pm 0.15$	$5.67 \pm 0.19$	–	–
	✗	✓	✓	$0.0129 \pm 0.247$	$0.458 \pm 0.782$	$5.69 \pm 1.65$	$7.14 \pm 1.90$	–	–
NOQ	✓	✓	✗	$0.0147 \pm 0.0011$	$3.17 \pm 0.21$	$2.66 \pm 0.14$	$5.63 \pm 0.14$	–	–
	✓	✗	✓	$0.0145 \pm 0.0011$	$3.22 \pm 0.22$	$2.61 \pm 0.15$	$5.66 \pm 0.19$	–	–
ALL	✓	✓	✓	$0.0148 \pm 0.0011$	$3.11 \pm 0.21$	$2.73 \pm 0.16$	$5.77 \pm 0.20$	$0.240 \pm 0.040$	–
NOQ	✓	✗	✓	$0.0145 \pm 0.0011$	$3.20 \pm 0.22$	$2.64 \pm 0.15$	$5.70 \pm 0.19$	$0.225 \pm 0.079$	–
ALL	✓	✓	✓	$0.0147 \pm 0.0011$	$3.16 \pm 0.20$	$2.67 \pm 0.15$	$5.65 \pm 0.18$	–	$2.70 \pm 1.39$
NOQ	✓	✗	✓	$0.0145 \pm 0.0012$	$3.23 \pm 0.23$	$2.61 \pm 0.15$	$5.69 \pm 0.19$	–	$3.85 \pm 2.70$
ALL*	✓	✓	✓	$0.0148 \pm 0.0012$	$3.10 \pm 0.21$	$2.72 \pm 0.16$	$5.77 \pm 0.19$	$0.25 \pm 0.05$	$3.61 \pm 1.08$

Notes. \*: priors on  $f_{\text{esc}}$  and  $C_{\text{HII}}$  are different for comparison with Price et al. (2016), see text for details

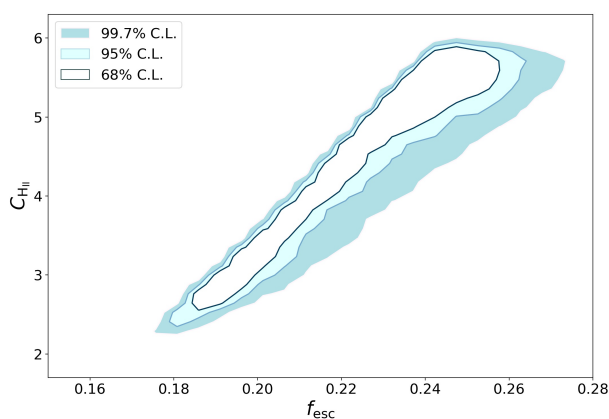


Fig. 8: MCMC distribution for  $f_{\text{esc}}$  and  $C_{\text{HII}}$  when both are taken as fit parameters (other parameters fixed). The escape fraction is allowed to vary between 0.1% and 100%, the clumping factor between 1 and 7.

Sec. 4.1, the resulting ionisation histories are also close to the ones observed on Fig. 3 and are hence in good agreement with observations.

Finally, we consider the case where the 4 parameters describing the evolution of  $\rho_{\text{SFR}}(z)$  are set free in the same time as  $f_{\text{esc}}$  and  $C_{\text{HII}}$ , using all datasets. We assume the same prior as Price et al. (2016) on  $C_{\text{HII}}$  considering values between 1 and 5. The full triangle plot is shown in Fig. A.3 and best fit parameters are reported in Table 3. The values found are in agreement with previous runs, with an undetermined value of  $C_{\text{HII}}$  at the  $2\sigma$  level. As in Price et al. (2016) the degeneracy between  $f_{\text{esc}}$  and  $C_{\text{HII}}$  and the current data do not allow to constrain strongly all free parameters. However the evolution of the filling factor (Fig. 9) and thus the derived value of  $\tau$  remain quite well constrained ( $\tau = 0.061 \pm 0.003$ ) and in agreement with Planck ( $\tau_{\text{Planck}} = 0.058 \pm 0.012$ ). Note however that the smaller envelope, as compared to Fig. 3, is mainly due to the constraints put by the filling factor data points.

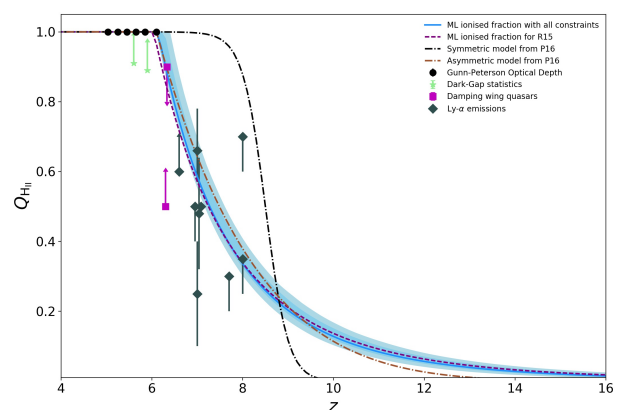


Fig. 9: Redshift evolution of  $Q_{\text{HII}}$  when all parameters ( $a, b, c, d, f_{\text{esc}}, C_{\text{HII}}$ ) are set free and all datasets used. Fig. A.3 show the corresponding constraints on assumed parameters.

## 5. Discussion

### 5.1. Influence of the magnitude limit

Values of SFR density with redshift are deduced from luminosity functions (LF) of star-forming galaxies. LF can be observed down to a certain magnitude, but need to be extrapolated if we want to consider the contribution of fainter galaxies. Indeed, the exact calculation of the comoving ionization rate  $\dot{n}_{\text{ion}}$  is given in Eq. 13, assuming that star-forming galaxies dominated the reionisation process. We chose in Sec. 2.1 to consider values of  $f_{\text{esc}}$  and  $\xi_{\text{ion}}$  averaged over the magnitude, i.e. effective values, hence the second line of Eq. 13 below:

$$\dot{n}_{\text{ion}} = \int_{M_{\text{lim}}}^{\infty} \phi(M_{\text{UV}}) f_{\text{esc}}(M_{\text{UV}}) \xi_{\text{ion}}(M_{\text{UV}}) dM_{\text{UV}} \quad (13)$$

$$\simeq \langle f_{\text{esc}} \xi_{\text{ion}} \rangle \int_{M_{\text{lim}}}^{\infty} \phi(M_{\text{UV}}) dM_{\text{UV}}. \quad (14)$$

We see that the choice of  $M_{\text{lim}}$  is fundamental. Bouwens et al. (2015) state that faint galaxies must contribute to the total UV radiation from galaxies but, assuming they do not form efficiently for lower luminosities (see Rees & Ostriker 1977; Mac Low & Ferrara 1999; Dijkstra et al. 2004), the authors choose to use  $M_{\text{lim}} = -13$  rather than  $M_{\text{lim}} = -17$ . We want to see how our results change if we use a different magnitude limit. To do so, we



Table 4: ML parameters for the fits on  $f_{\text{esc}}(z)$  and  $C_{\text{HII}}(z)$  in, respectively, Sec. 4.2 and 4.3.

Model	Reference	$Q_{\text{HII}}$	$\tau_{\text{Planck}}$	Model parameters			
$f_{\text{esc}}(z)$	KFG12	✓	✓	$\alpha$	$\beta$		
		✓	✗	$0.17 \pm 0.02$	$0 \pm 0.23$		
		✗	✓	$0.18 \pm 0.02$	$0 \pm 0.24$		
				$0.12 \pm 0.09$	$0.66 \pm 0.76$		
$C_{\text{HII}}(z)$	HM12.1	✓	✓	$\alpha$	$a$	$b$	$c$
		✓	✗	$0.74 \pm 0.81$	$-2.38 \pm 1.34$	$4.06 \pm 1.02$	–
	HM12.2	✓	✗	$0.85 \pm 0.84$	$-2.33 \pm 1.28$	$3.93 \pm 1.08$	–
		✓	✓	$0.75 \pm 0.77$	$0 \pm 0.29$	$-0.27 \pm 0.14$	$4.12 \pm 0.99$
		✓	✗	$0.90 \pm 0.79$	$0 \pm 0.30$	$-0.25 \pm 0.13$	$3.94 \pm 1.01$
I07	✓	✓	–	$4.96 \pm 0.44$	$-0.073 \pm 0.036$	$0 \pm 3.8 \times 10^{-4}$	
	✓	✗	–	$4.89 \pm 0.44$	$-0.079 \pm 0.041$	$0 \pm 4.7 \times 10^{-5}$	

**References.** KFG12: Kuhlen & Faucher-Giguère (2012); HM12.1 & HM12.2: Haardt & Madau (2012); I07: Iliev et al. (2007).

follow the steps of Ishigaki et al. (2015), using the luminosity functions computed by the authors, as well as the corresponding model for  $\rho_{\text{UV}}(z)$ :

$$\rho_{\text{UV}}(z) = \frac{2\rho_{\text{UV}}(z=8)}{10^{a(z-8)} + 10^{b(z-8)}}. \quad (15)$$

Here,  $\rho_{\text{UV}}(z=8)$  is a normalisation factor, and  $a$  and  $b$  determine the slope of  $\rho_{\text{UV}}(z)$ . This model is designed to reproduce the rapid decrease of  $\rho_{\text{UV}}(z)$  from  $z \sim 8$  towards high redshifts and does not consider the bump on luminosity density we observe at redshifts  $z < 4$ . We adopt this model into a Monte Carlo Markov Chain approach similar to Sec. 4. We fit to the UV luminosity densities from Ishigaki et al. (2015), to filling factor data points, and to  $\tau_{\text{Planck}}$ , both for  $M_{\text{lim}} = -17$  and  $M_{\text{lim}} = -10$ . Results for the two magnitude limits studied can be found in Fig. 11. We see the distribution of possible scenarii is quite spread with the 95% confidence interval drawn on the figure. In both cases, the effect of the two additional sets of data used as constraints here,  $Q_{\text{HII}}$  and  $\tau_{\text{Planck}}$ , which were not used in Ishigaki et al. (2015), is to lower the quantity of ionising sources needed at high redshift to achieve a complete reionisation of the IGM by  $z \sim 6.5$ .

We compute the reionisation history compatible with the three sets of observational data, for the maximum likelihood parameters (here, median values) of the parametrisation in Eq. 15 for the two  $M_{\text{lim}}$  values and compare them to previous results – where  $M_{\text{lim}} = -13$ . Results can be seen on Fig. 10. It is important to note that values of other parameters, not considered in the fit, were taken from Ishigaki et al. (2015) and hence quite different from the ones used in Sec. 4.1. Particularly, the value of the clumping factor was found by Ishigaki et al. to be 1.9 for  $M_{\text{lim}} = -17$  and 1.0 for  $M_{\text{lim}} = -10$  – recall we used  $C_{\text{HII}} = 3$  before. Hence this analysis gives an idea of the systematic uncertainties on reionisation history due to the choice of the magnitude limit, but also of  $f_{\text{esc}}$  and  $C_{\text{HII}}$ . We see these are much wider than the statistical uncertainties observed at first on Fig. 3 but still reasonable and in particular, they mainly concern a range of redshift where data points are still missing: we may expect that once data on earlier times is available, it will strongly constrain the magnitude limit value choice. In this perspective we can mention the work of Mason et al. (2017), who derived a new constrain on reionisation history from simulations and models of the effects of ISM radiative transfer on Lyman- $\alpha$  emissions. They find an ISM ionised fraction at  $z \sim 7$  of  $x_{\text{HII}} = 0.41_{-0.11}^{+0.15}$  in better agreement with our model for  $M_{\text{lim}} = -17$  (see Fig. 10).

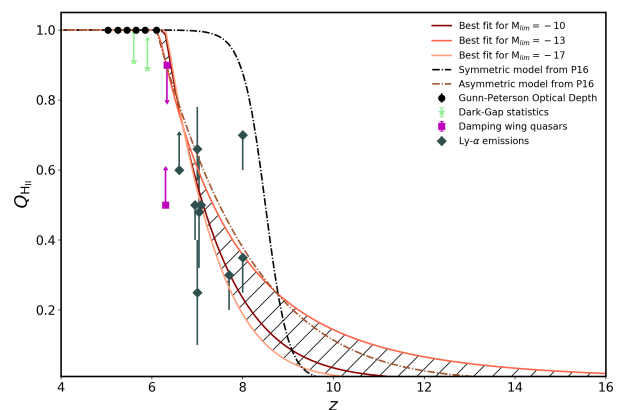


Fig. 10: Redshift evolution of  $Q_{\text{HII}}$  for various choices of the magnitude limit in luminosity data: brown for  $M_{\text{lim}} = -10$ , orange for  $M_{\text{lim}} = -13$  and beige for  $M_{\text{lim}} = -17$ . The hatched region represents the systematic uncertainties due to the choice of the magnitude limit.

From a different point of view, Price et al. (2016) consider a varying value of  $M_{\text{lim}}$  with redshift, and find that  $M_{\text{lim}}$  varies in order to match the value of  $\tau_{\text{Planck}}$  and to balance the increasing value of  $f_{\text{esc}}$  with redshift authorised in their model.

## 5.2. How are $f_{\text{esc}}$ , $\dot{n}_{\text{ion}}$ and $\rho_{\text{SFR}}$ correlated?

We expect a correlation between the amplitude  $a$  of the star formation rate density parametrisation Eq. 2 and the escape fraction. Indeed,  $f_{\text{esc}}$  takes no part in the estimation of  $\rho_{\text{SFR}}$  but intervenes in the same equations: the calculation of  $\dot{n}_{\text{ion}}$  in Eq. 1 and then the integration of  $Q_{\text{HII}}$  in Eq. 3. Thus, we can infer that they are constrained by the same data, so that the PDF of parameter  $a$  can translate both  $a$  and  $f_{\text{esc}}$  variations when the escape fraction is set to 0.2. To investigate this possible correlation, we plot the distributions of  $a \times f_{\text{esc}}$  for various sets of constraints and in different models: with (PAR) and without (CST) the escape fraction as a fifth fit parameter and with all constraints (ALL), without  $\rho_{\text{SFR}}$  constraints (NORHO) and with only  $\rho_{\text{SFR}}$  constraints (RHO) considered in the fit. It is nevertheless difficult to proceed to a detailed comparison of the parameter distributions and constraints they are related to. Indeed,  $a$  and  $f_{\text{esc}}$  share the same equations but the one

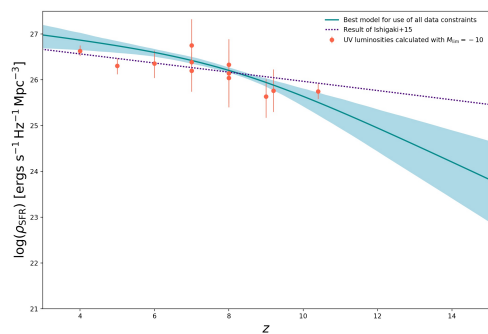
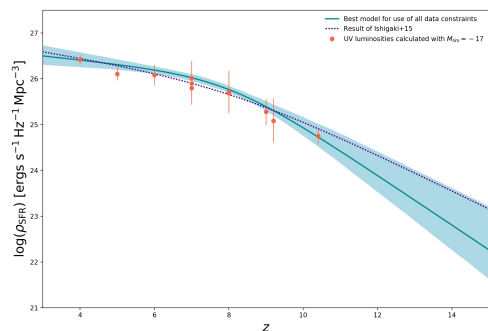

(a)  $M_{\text{lim}} = -10$ 

(b)  $M_{\text{lim}} = -17$ 

Fig. 11: UV luminosity density  $\rho_{\text{UV}}$  with redshift in logarithmic scale. Data points are from Ishigaki et al. (2015). Maximum likelihood parametrizations (continuous lines) are shown for fits using all observational constraints: data on the figures,  $Q_{\text{HII}}$  data and  $\tau_{\text{Planck}}$ . The 95% confidence interval on  $\rho_{\text{UV}}$  corresponds to the light blue region. These results are compared with a model forced to reproduce results from Ishigaki et al. (2015) drawn as the purple dotted line.

where  $\rho_{\text{SFR}}$  is computed. However, as seen in Sec. 4.1, the star formation history is also the most constraining data so that parameter distributions are extremely spread when they are skipped (see Table 3). We therefore cannot accurately compare **NORHO** results with others and choose to compare median values of  $a \times f_{\text{esc}}$  distributions rather than their shapes. We find that **CST** gives a lower value than **PAR** with a relative difference of 16.6% for **ALL** and of 19.2% for **RHO**. We can hardly conclude on a correlation between  $a$  and  $f_{\text{esc}}$ : it seems that other parameters impact the value of the escape fraction, preventing the correlation.

To further investigate the link between  $f_{\text{esc}}$ ,  $\dot{n}_{\text{ion}}$  and  $\rho_{\text{SFR}}$ , we consider values of the reionisation rate at various redshifts, used in Kuhlen & Faucher-Giguère (2012) and Robertson et al. (2013), and inferred from measurements and calculations of Faucher-Giguère et al. (2008); Prochaska et al. (2009); Songaila & Cowie (2010). We call **NION** the run using these new constraints – in addition to the others – and **FREE** the one skipping them, corresponding to **ALL** from Sec. 4.2.

We compare in Table 5 values of the reionisation rate at various redshifts for **NION**, **FREE** and Kuhlen & Faucher-Giguère (2012). **NION** gives results close to data points, increasing with  $z$ , whereas **FREE** values are significantly higher and decrease with redshift. This difference in the evolutions of  $\dot{n}_{\text{ion}}(z)$  is di-

Table 5: Comparison between our results and data points on the cosmic reionisation rate from Kuhlen & Faucher-Giguère (2012).

$z$	$\dot{n}_{\text{ion}} [ 10^{50} \text{ s}^{-1} \text{ Mpc}^{-3} ]$		
	KFG12	NION	FREE
4.0	$3.2^{+2.2}_{-1.9}$	4.50	16.7
4.2	$3.5^{+2.9}_{-2.2}$	4.54	15.4
5.0	$4.3 \pm 2.6$	4.66	11.3

References. KFG12: Kuhlen & Faucher-Giguère (2012).

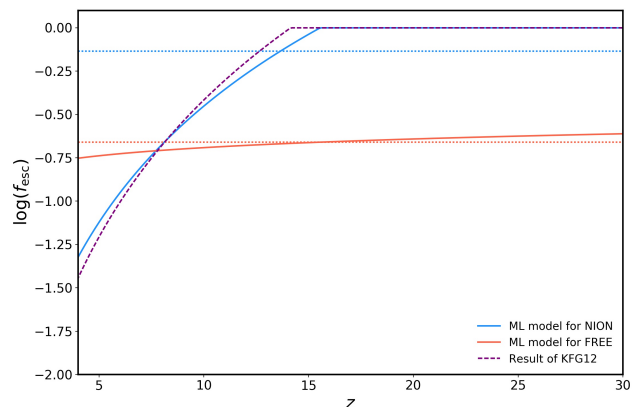


Fig. 12: Evolution of  $f_{\text{esc}}$  with redshift when  $\dot{n}_{\text{ion}}$  data points are used. ML models are shown for various set of constraints: blue when all constraints are used (**NION**); coral when  $\dot{n}_{\text{ion}}$  constraints are skipped (**FREE**). Horizontal dashed lines represent the mean value of  $f_{\text{esc}}$  over  $4 \leq z \leq 30$  for the model of the corresponding colour. Inferences are compared to results of Kuhlen & Faucher-Giguère (2012, KFG12, purple dashed line).

rectly linked to  $f_{\text{esc}}(z)$ . For instance,  $f_{\text{esc, FREE}}$  is almost constant with redshift (coral solid line in Fig. 12) and  $\dot{n}_{\text{ion}}(z)$  follows therefore the evolution of  $\rho_{\text{SFR}}(z)$  which decreases on this redshift range (see Eq. 1). On the contrary, to satisfy both the low  $\dot{n}_{\text{ion}}$  values and the very constraining star formation data,  $f_{\text{esc, NION}}$  has to take low values at low  $z$ , as can be seen on Fig. 12 (blue solid line). Then, to allow reionisation to end at  $z \sim 6$  (filling factor constraints) despite the fact that there are fewer sources and that only few ionising photons escape from galaxies at low redshift,  $f_{\text{esc}}$  must increase: it quickly reaches 1, where it saturates. Such a behaviour of  $f_{\text{esc}}$  implies that reionisation starts early with high efficiency, leading to a high value of  $\tau = 0.095$ , outside the  $3\text{-}\sigma$  confidence interval of  $\tau_{\text{Planck}}$  and therefore hardly compatible with Planck Collaboration et al. (2016b). Removing the constraints on the filling factor,  $f_{\text{esc}}$  remains low on the whole redshift range ( $< 20$ ). We then get values of the optical depth in agreement with Planck ( $0.058 \pm 0.011$ ) but reionisation does not end before  $z \sim 4$ . Thus, the estimations on the reionisation rate from Faucher-Giguère et al. (2008); Prochaska et al. (2009); Songaila & Cowie (2010) are compatible with one observable at a time: either the ionisation level – leading to a higher value of  $\tau$  –, or the Thomson optical depth – so that reionisation ends around  $z \sim 4$  –, but cannot match all observations in a coherent way.

### 5.3. Reionisation sources at $z > 10$

Some doubts remain about the sources of reionisation: if [Robertson et al. \(2015\)](#) found that star-forming galaxies are sufficient to lead the process and to maintain the IGM ionised at  $z \sim 7$  – assuming  $C_{\text{HII}} = 3$  and  $f_{\text{esc}} = 0.2$ , their analysis extrapolates luminosity functions between  $z \simeq 10$  and  $z \simeq 30$ , overlooking the possibility that other sources may have taken part in the early stages of reionisation process. Besides, they argue that low values of the Thomson optical depth reduce the need for a significant contribution of high-redshift galaxies and [Planck Collaboration et al. \(2016b\)](#) give much lower values than WMAP did ([Hinshaw et al. 2013](#)):  $\tau_{\text{Planck}} = 0.058 \pm 0.012$  vs.  $\tau_{\text{WMAP}} = 0.088 \pm 0.014$ . Thus, now that we have investigated the possibility of this extrapolation, we choose to try the one of a constant SFR at  $z \gtrsim 10$ .

We perform an MCMC maximum likelihood sampling of the 4-parameter model of  $\rho_{\text{SFR}}(z)$  in Eq. 2 and add as a fifth parameter the value of SFR density at  $z > 10.4$ , our last data point corresponding to a redshift of 10.4. We call it  $\rho_{\text{asympt}}$  and choose to use all observations cited in Sec. 2.1 as constraints. Final values of parameters  $a$ ,  $b$ ,  $c$  and  $d$  are close to the ones from Sec. 4.1. We find that there is a strong correlation between  $\rho_{\text{asympt}}$  and  $\tau$ , because of the direct integration in Eq. 7 and so expect higher values of the optical depth for high values of  $\rho_{\text{asympt}}$ . Yet, because of the very constraining power of the ionisation level at  $5 \lesssim z \lesssim 7$  ([Fan et al. 2006](#)),  $\tau$  values are limited and there is actually more impact on the global storyline. Indeed, models where  $Q_{\text{HII}}$  equals 30% as soon as  $z = 10$  are allowed, whereas it is closer to 20% at the same redshift when  $\rho_{\text{SFR}}$  is extrapolated. The correlation observed in our model parameters likelihood functions between  $\rho_{\text{asympt}}$  and  $\tau$  had already been noticed by [Robertson et al. \(2015\)](#), as a correlation between  $\tau$  and the averaged value of  $\rho_{\text{SFR}}$  for  $z > 10$ . A linear regression gives

$$\langle \rho_{\text{SFR}} \rangle_{z > 10.4} = 0.53 \tau - 0.029 [\text{M}_{\odot} \text{yr}^{-1} \text{Mpc}^{-3}], \quad (16)$$

with a correlation coefficient  $r = 0.993$ .

In this parametrisation,  $\rho_{\text{asympt}}$  can take very low values (down to  $10^{-5} [\text{M}_{\odot} \text{yr}^{-1} \text{Mpc}^{-3}]$ ) meaning that reionisation sources are almost completely absent at  $z > 10$ . It also has an upper limit of  $0.016 [\text{M}_{\odot} \text{yr}^{-1} \text{Mpc}^{-3}]$ . This is close to the redshift-independent evolution of  $\rho_{\text{SFR}}$  ( $\simeq 10^{-1.5} [\text{M}_{\odot} \text{yr}^{-1} \text{Mpc}^{-3}]$ ) considered by [Ishigaki et al. \(2015\)](#) for  $z > 3$  in order to reproduce  $\tau_{2014} = 0.091^{+0.013}_{-0.014}$  ([Planck Collaboration et al. 2014](#)), when usual decreasing models only gave them  $\tau \simeq 0.05$ . We can compare Sec. 4.1 results with this upper limit on Figure 2. Besides, despite the wide range of possible values for  $\rho_{\text{asympt}}$ , all results are consistent with our data: optical depths always remain in the 68% confidence interval of  $\tau_{\text{Planck}}$  and reionisation is always ended by  $z = 6$ .

## 6. Conclusions

We used the latest observational data available on reionisation history, i.e. cosmic star formation density, ionised fraction of the IGM and Thomson optical depth derived from Planck observations to find that they are all compatible with a simple and credible storyline where reionisation begins around  $z = 15$  and ends by  $z = 6$ . Among all data, star formation history seems to be the most constraining for the EoR.

An investigation of various parametrisations of the escape fraction of ionising photons has lead us to conclude that it is very well constrained by observations: when considered constant

with redshift, values allowed by the fit range from 20% to 28%; when considered redshift-dependent, from  $f_{\text{esc}}(z = 4) \simeq 17\%$  to  $f_{\text{esc}}(z = 30) \simeq 26\%$  following a low increase with  $z$ . The fiducial constant value of 20% often used in papers seems then to be perfectly consistent with our data.

On the contrary, the clumping factor of ionised hydrogen in the IGM can take a wide range of different values without impacting the reionisation observables significantly. For instance, when take  $C_{\text{HII}}$  as a redshift-independent parameter, its relative standard deviation is 51.5% whereas it is at most 3.4% for  $Q_{\text{HII}}(z)$ <sup>3</sup>. The result is the same when we consider that  $C_{\text{HII}}$  depends on redshift: a great variety of possible evolutions gives the same storyline in terms of ionisation level. There is no greater impact on Thomson optical depth values, which vary of a maximum of a few percent compared to  $\langle \tau \rangle_{C_{\text{HII}}=3}$  and always remains in the 1- $\sigma$  confidence interval of  $\tau_{\text{Planck}}$ . Observational constraints are thus extremely robust to variations of the clumping factor. We nevertheless find a correlation between the averaged value of  $C_{\text{HII}}$  for  $z \in [6.8, 30]$  and  $\tau$ : the linear fit

$$\langle C_{\text{HII}} \rangle_{z > 6.8} = -460 \tau + 31.5 \quad (17)$$

provides a good description of their connection. This supports the use of a redshift-independent clumping factor to study the EoR. A possible choice, consistent with observations, would then be  $C_{\text{HII}} = 3$ , the fiducial value often used in papers, because it lies in the range [2.0, 4.5] of the mean values for  $C_{\text{HII}}$  found in Sec. 4.3.

Last, a quick study on the possible reionisation sources at  $z \gtrsim 10$  showed that there is no need for exotic sources as early quasars ([Madau & Haardt 2015](#)) or for an artificial increase in star formation density at high redshift ([Ishigaki et al. 2015](#)). When their luminosity functions are extrapolated, a hypothesis still recently strongly supported by [Livermore et al. \(2017\)](#), star-forming galaxies provide enough photons to have a fully ionised IGM at  $z = 6$ .

*Acknowledgements.* The authors thank B.E. Robertson for kindly providing us with his compilation of star formation rate densities. This research made use of Astropy, a community-developed core Python package for Astronomy (Astropy Collaboration et al. 2013) and matplotlib, a Python library for publication quality graphics (Hunter 2007). This work was partly supported by Programme National de Cosmologie et Galaxies (PNCG).

<sup>3</sup> Reached at  $z = 6.3$ .

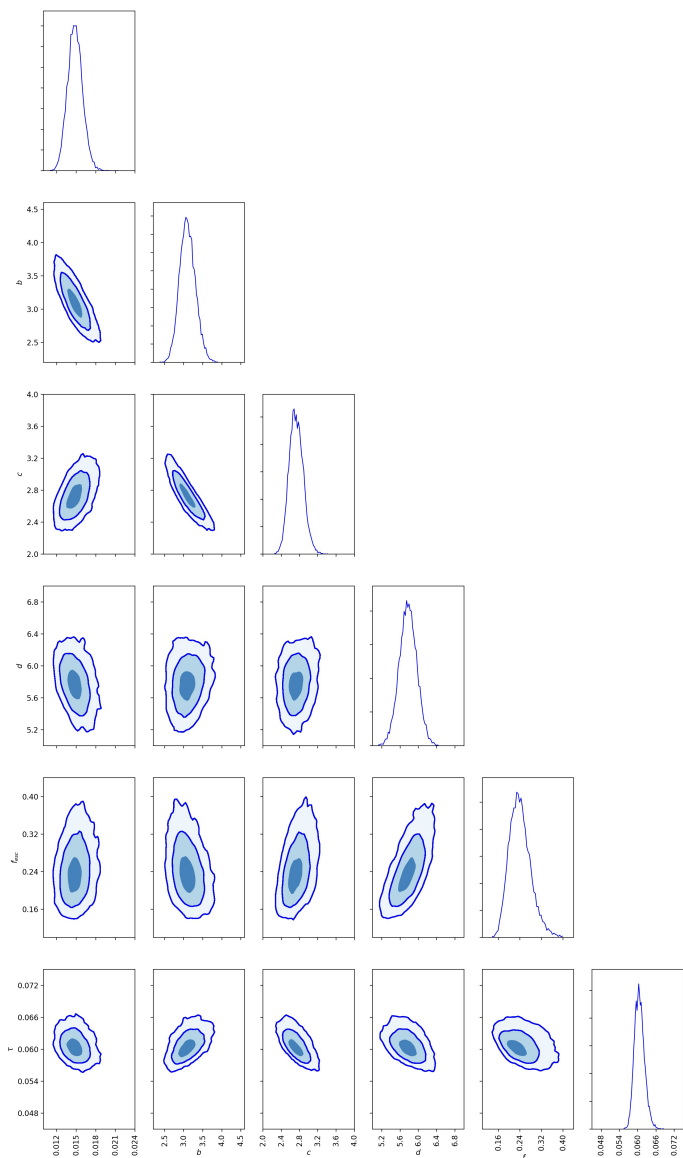


Fig. A.1: Results of the MCMC analysis for the ALL case when  $f_{esc}$  is added as a free parameter. The contours show the 1, 2, 3  $\sigma$  confidence levels for  $a$ ,  $b$ ,  $c$ ,  $d$ ,  $f_{esc}$  and the derived parameter  $\tau$ .

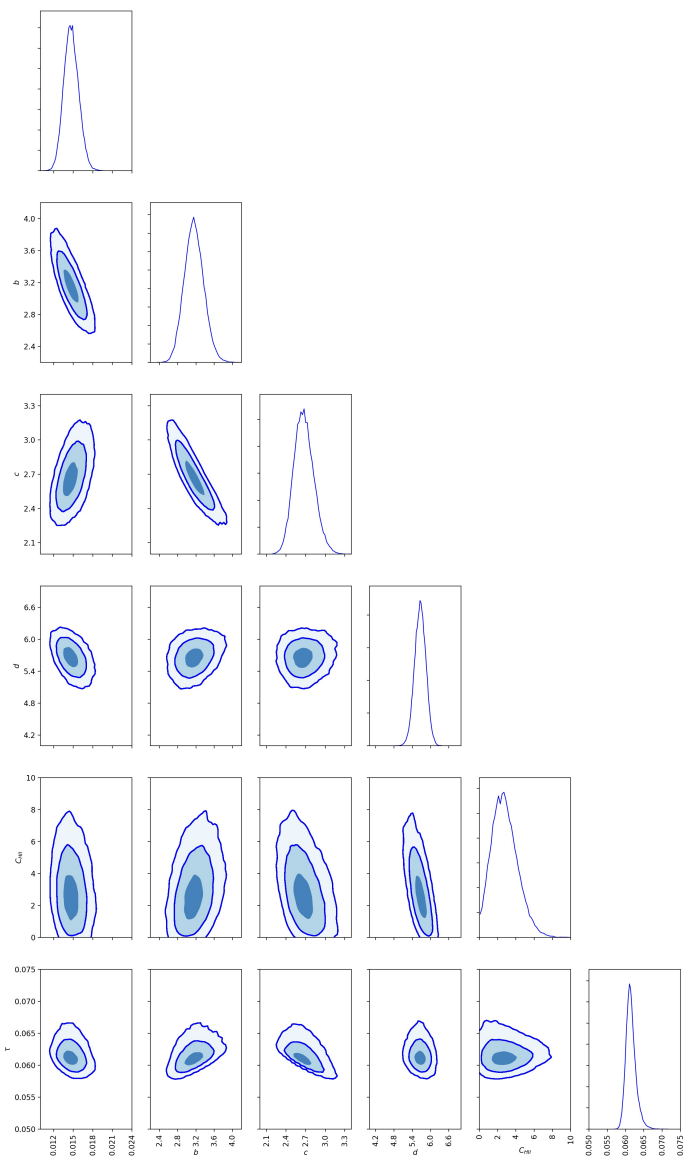


Fig. A.2: Results of the MCMC analysis for the ALL case when  $C_{HII}$  is added as a free parameter. The contours show the 1, 2, 3  $\sigma$  confidence levels for  $a$ ,  $b$ ,  $c$ ,  $d$ ,  $C_{HII}$  and the derived parameter  $\tau$ .

## Appendix A: MCMC multidimensional plots

We show in appendix the additional triangle plots of the runs ALL corresponding to the studies with  $f_{esc}$  as additional free parameter (see Section 4.1), with  $C_{HII}$  as additional free parameter (see Section 4.3), and finally with both free (see Section 4.4).

## References

- Aghanim, N., Desert, F. X., Puget, J. L., & Gispert, R. 1996, A&A, 311, 1  
Atek, H., Richard, J., Kneib, J.-P., et al. 2015, ApJ, 800, 18  
Becker, G. D., Bolton, J. S., Haehnelt, M. G., & Sargent, W. L. W. 2011, MNRAS, 410, 1096  
Becker, G. D., Bolton, J. S., Madau, P., et al. 2015, MNRAS, 447, 3402  
Bolton, J. S., Becker, G. D., Raskutti, S., et al. 2012, MNRAS, 419, 2880  
Bolton, J. S. & Haehnelt, M. G. 2007, MNRAS, 382, 325  
Bouwens, R. J., Illingworth, G. D., Oesch, P. A., et al. 2015, ApJ, 811, 140  
Bouwens, R. J., Illingworth, G. D., Oesch, P. A., et al. 2012, ApJ, 752, L5

- Dijkstra, M., Haiman, Z., Rees, M. J., & Weinberg, D. H. 2004, The Astrophysical Journal, 601, 666  
Douspis, M., Aghanim, N., Ilić, S., & Langer, M. 2015, A&A, 580, L4  
Dunlop, J. S., Rogers, A. B., McLure, R. J., et al. 2013, MNRAS, 432, 3520  
Fan, X., Strauss, M. A., Becker, R. H., et al. 2006, AJ, 132, 117  
Faucher-Giguère, C.-A., Lidz, A., Hernquist, L., & Zaldarriaga, M. 2008, ApJ, 688, 85  
Fernandez, E. R., Dole, H., & Iliev, I. T. 2013, ApJ, 764, 56  
Finkelstein, S. L., Ryan, Jr., R. E., Papovich, C., et al. 2015, ApJ, 810, 71  
Finlator, K., Oh, S. P., Özel, F., & Davé, R. 2012, MNRAS, 427, 2464  
Furlanetto, S. R. & Oh, S. P. 2005, MNRAS, 363, 1031  
Greig, B. & Mesinger, A. 2017, MNRAS, 465, 4838  
Gunn, J. E. & Peterson, B. A. 1965, ApJ, 142, 1633  
Haardt, F. & Madau, P. 2012, ApJ, 746, 125  
Hinshaw, G., Larson, D., Komatsu, E., et al. 2013, ApJS, 208, 19  
Hui, L. & Haiman, Z. 2003, ApJ, 596, 9  
Iliev, I. T., Mellema, G., Pen, U.-L., et al. 2006, MNRAS, 369, 1625  
Iliev, I. T., Mellema, G., Shapiro, P. R., & Pen, U.-L. 2007, MNRAS, 376, 534  
Ishigaki, M., Kawamata, R., Ouchi, M., et al. 2015, ApJ, 799, 12  
Iwata, I., Inoue, A. K., Matsuda, Y., et al. 2009, ApJ, 692, 1287  
Kuhlen, M. & Faucher-Giguère, C.-A. 2012, MNRAS, 423, 862

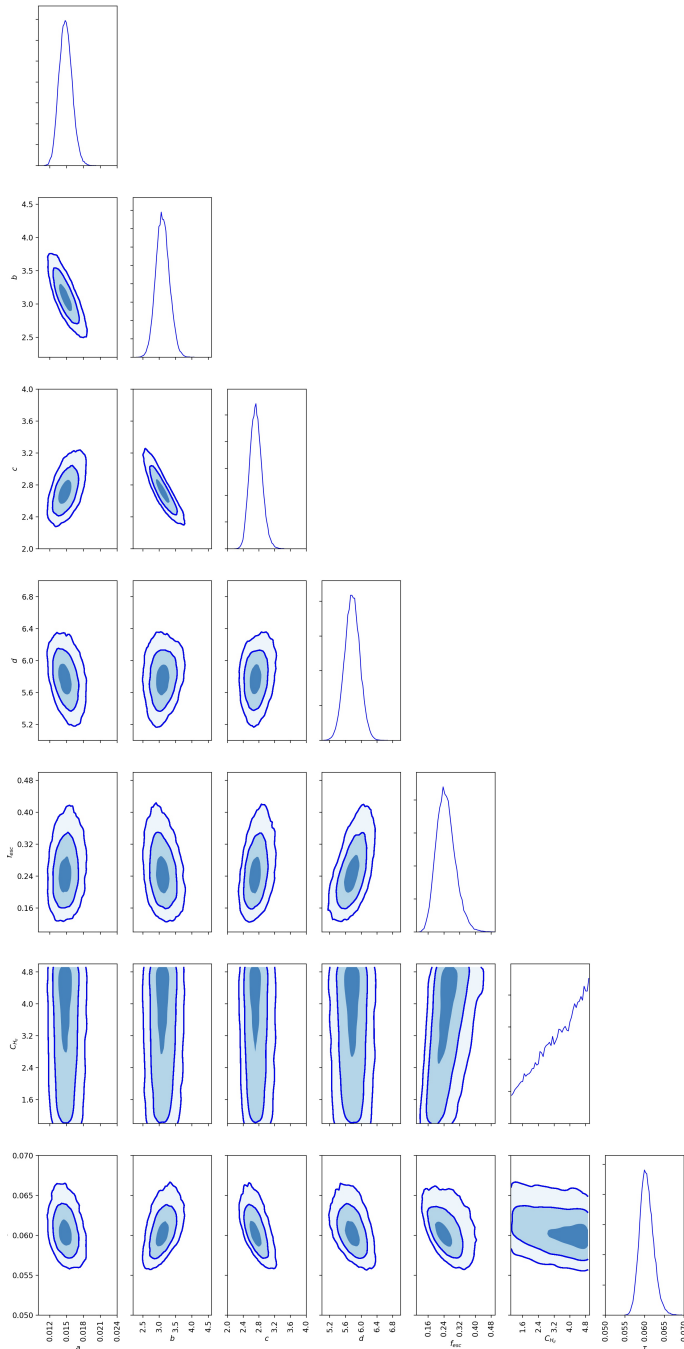


Fig. A.3: Results of the MCMC analysis for the ALL case when both  $f_{esc}$  and  $C_{HII}$  are added as a free parameter. The contours show the 1, 2, 3  $\sigma$  confidence levels for a, b, c, d,  $f_{esc}$ ,  $C_{HII}$  and the derived parameter  $\tau$ .

Lidz, A., Faucher-Giguère, C.-A., Dall’Aglio, A., et al. 2010, ApJ, 718, 199  
Livermore, R. C., Finkelstein, S. L., & Lotz, J. M. 2017, ApJ, 835, 113  
Loeb, A. & Furlanetto, S. 2013, The First Galaxies in the Universe (Princeton University Press)  
Mac Low, M.-M. & Ferrara, A. 1999, ApJ, 513, 142  
Madau, P. & Dickinson, M. 2014, ARA&A, 52, 415  
Madau, P. & Haardt, F. 2015, ApJ, 813, L8  
Mason, C. A., Treu, T., Dijkstra, M., et al. 2017, ArXiv e-prints [arXiv:1709.05356]  
McGreer, I. D., Mesinger, A., & D’Odorico, V. 2015, MNRAS, 447, 499  
McLeod, D. J., McLure, R. J., Dunlop, J. S., et al. 2015, MNRAS, 450, 3032  
McLure, R. J., Dunlop, J. S., Bowler, R. A. A., et al. 2013, MNRAS, 432, 2696  
Mellema, G., Iliev, I. T., Pen, U.-L., & Shapiro, P. R. 2006, MNRAS, 372, 679

Mesinger, A., ed. 2016, Astrophysics and Space Science Library, Vol. 423, Understanding the Epoch of Cosmic Reionization  
Oesch, P. A., Bouwens, R. J., Ilingworth, G. D., et al. 2015, ApJ, 808, 104  
Osterbrock, D. E. 1989, Astrophysics of gaseous nebulae and active galactic nuclei (University Science Books)  
Paardekooper, J.-P., Khochfar, S., & Dalla Vecchia, C. 2015, MNRAS, 451, 2544  
Pawlik, A. H., Schaye, J., & van Scherpenzeel, E. 2009, MNRAS, 394, 1812  
Peebles, P. J. E. 1968, ApJ, 153, 1  
Planck Collaboration et al. 2014, A&A, 571, A16  
Planck Collaboration et al. 2016a, A&A, 594, A13  
Planck Collaboration et al. 2016b, A&A, 596, A108  
Price, L. C., Trac, H., & Cen, R. 2016, ArXiv e-prints [arXiv:1605.03970]  
Prochaska, J. X., Worseck, G., & O’Meara, J. M. 2009, ApJ, 705, L113  
Raičević, M. & Theuns, T. 2011, MNRAS, 412, L16  
Rees, M. J. & Ostriker, J. P. 1977, MNRAS, 179, 541  
Robertson, B. E., Ellis, R. S., Furlanetto, S. R., & Dunlop, J. S. 2015, ApJ, 802, L19  
Robertson, B. E., Furlanetto, S. R., Schneider, E., et al. 2013, ApJ, 768, 71  
Schenker, M. A., Robertson, B. E., Ellis, R. S., et al. 2013, ApJ, 768, 196  
Schroeder, J., Mesinger, A., & Haiman, Z. 2013, MNRAS, 428, 3058  
Seager, S., Sasselov, D. D., & Scott, D. 2000, ApJS, 128, 407  
Shull, J. M., Harness, A., Trenti, M., & Smith, B. D. 2012, ApJ, 747, 100  
Sobacchi, E. & Mesinger, A. 2014, MNRAS, 440, 1662  
Sokasian, A., Abel, T., Hernquist, L., & Springel, V. 2003, MNRAS, 344, 607  
Songaila, A. & Cowie, L. L. 2010, ApJ, 721, 1448  
Steidel, C. C., Pettini, M., & Adelberger, K. L. 2001, ApJ, 546, 665  
Strömgren, B. 1939, ApJ, 89, 526  
Wise, J. H., Demchenko, V. G., Halicek, M. T., et al. 2014, MNRAS, 442, 2560  
Yajima, H., Li, Y., Zhu, Q., et al. 2014, MNRAS, 440, 776  
Yoshiura, S., Hasegawa, K., Ichiki, K., et al. 2017, MNRAS, 471, 3713  
Zel’dovich, Y. B., Kurt, V. G., & Syunyaev, R. A. 1969, Soviet Journal of Experimental and Theoretical Physics, 28, 146